Applied Catalysis A: General 466 (2013) 161–168

Contents lists available at SciVerse ScienceDirect

Applied Catalysis A: General

journal homepage: www.elsevier.com/locate/apcata

Hydrogenolysis of cellulose into polyols over Ni/W/SiO_2 catalysts

Su Jin You, In Gu Baek, Eun Duck Park*

Division of Energy Systems Research and Department of Chemical Engineering, Ajou University, San 5 Woncheon-dong, Yeongtong-gu, Suwon, 443-749, Republic of Korea

ARTICLE INFO

Article history:
Received 22 February 2013
Received in revised form 26 May 2013
Accepted 29 June 2013
Available online 8 July 2013

Keywords:
Cellulose
Ethylene glycol
Hydrogenolysis
NiW
Silica

ABSTRACT

The direct conversion of cellulose into polyols in the presence of hydrogen was examined over Ni/W/SiO_2 catalysts to establish the effects of average pore size of support and reduction temperature on the catalytic performance. The crystalline particle size of W, determined by X-ray diffraction (XRD), generally increased with increase in the average pore size of support and reduction temperature for Ni/W/SiO_2. The yield of polyols such as sorbitol, mannitol, erythritol, ethylene glycol, and 1,2-propanediol increased on decreasing the crystalline particle size of W in Ni/W/SiO_2. The individual catalytic activity of Ni/W/SiO_2 was much better than that of the combined catalyst systems, i.e., Ni/SiO_2 + W and Ni/SiO_2 + WO_3. The oxidation state effect of nickel and tungsten in Ni/W/SiO_2 catalyst on the catalytic performance was also investigated. The reduced and oxidized Ni/W/SiO_2 catalysts were found to be effective in forming polyols and organic acids, respectively.

1. Introduction

Increasing fossil fuel prices because of limited reservoirs and the increase in the atmospheric CO_2 concentration owing to fossil fuel consumption have stimulated a greater interest in utilizing biomass for sustainable production of energy and chemicals. Cellulose, one of the most abundant resources of biomass, typically comprises 40–50% of the terrestrial biomass and does not directly compete with the food supply chain. Cellulose has a crystalline and robust structure and cannot be easily hydrolyzed to its monomer as compared to starch because of the β-1,4 linkages of D-glucopyranose monomers and hydrogen bond [1]. A key challenge for effective cellulose utilization is its transformation into valuable chemicals, including glucose, polyols, 5-hydroxymethylfurfural, oil, organic acids, and gaseous hydrocarbons [1–3].

Recently, much attention has been paid to the one-pot conversion of cellulose into polyols (alcohols containing multiple hydroxyl groups), which are important intermediates in the manufacture of perfumes, beer, pharmaceuticals, polyesters, polyethers, and polyurethanes. The pioneering work of Fukuoka and Dhepe [4] has led to the investigation of various catalyst systems for hydrogenolysis of cellulose [4–26] such as Pt/γ-Al_2O_3 [4], Pt/H-ZSM-5 [5], Pt/carbon black [6], Pt/MCM-48 [7], Ru/C [8], Ru/carbon nanotubes [9,10], Ru/$Cs_3PW_{12}O_{40}$ [11], heteropolyacids combined with Ru/C [12,13], mineral acid combined with Ru/C [14,15], mineral acid combined with Ru/USY [16], and Ru/C combined with WO_3 and tungstic acid [17,18]. Besides the expensive noble metal catalysts, nonnoble metal catalysts such as Ni- and W-based catalysts have also been reported to be quite active in the cellulose hydrogenolysis reaction [19–21]. These include Ni supported on ZnO, Al_2O_3, SiO_2, TiO_2, activated carbon, MgO, and H-ZSM-5 [22,23], Ni-Ir/activated carbon [24], Ni_2P/activated carbon [25], Ni/W/SiO_2-Al_2O_3 [26], Ni-W_2C/activated carbon [19], Ni-W_xC/CMK-3 [20], and Ni-W/SBA-15 [21]. Zhang and co-workers reported that up to 62% of ethylene glycol yield could be obtained using W-based catalysts under optimized reaction conditions (518 K, 6 MPa H_2) [19–21]. However, despite their outstanding catalytic performance, limited work has been reported on the supported NiW catalysts [21,26].

In this work, the effect of certain factors (physical properties of the support and reduction degree of supported metals) on the catalytic performance for the reaction over NiW/SiO_2 is investigated. The average pore diameter of SiO_2 support and the reduction temperature affect the crystalline particle size of W, resulting in different catalytic activities. Furthermore, the oxidation states of Ni and W also determine the product distribution.

2. Experimental

2.1. Catalyst preparation

Silica with various average pore diameters (denoted as SiO_2, pore size in Å) viz. SiO_2 (Zeochem, ZEOprep 40, S_{BET} = 629 m^2/g), SiO_2 (Zeochem, ZEOprep 60, S_{BET} = 542 m^2/g), SiO_2 (Zeochem, ZEOprep 90, S_{BET} = 434 m^2/g), and SiO_2 (Zeochem, ZEOprep 300, S_{BET} = 116 m^2/g) were purchased and utilized as supports after calcination in air at 973 K. The Ni/W/SiO_2 catalysts were prepared

* Corresponding author. Tel.: +82 31 219 2384; fax: +82 31 219 1612.
E-mail address: edpark@ajou.ac.kr (E.D. Park).

0926-860X/$ – see front matter © 2013 Elsevier B.V. All rights reserved.
http://dx.doi.org/10.1016/j.apcata.2013.06.053

Table 1
Physicochemical properties of Ni/W/SiO_2 with different average pore sizes.

Catalyst	Ni composition (wt.%)[a]	W composition (wt.%)[a]	BET surface area (m^2/g)	Amount of desorbed NH_3 (μmol NH_3/g)[b]	Particle size (nm)[c]	
					W	β-W
Ni/W/SiO_2(40)	4.0	31.5	184	78.5	15.5	11.7
Ni/W/SiO_2(60)	4.9	23.4	256	77.4	17.0	11.0
Ni/W/SiO_2(90)	4.9	24.0	234	46.7	17.8	10.0
Ni/W/SiO_2(300)	4.8	24.9	51	15.9	23.3	10.6

[a] The bulk composition was analyzed by ICP-AES.
[b] The total acidity was determined by quantifying the desorbed NH_3 by NH_3- TPD.
[c] The primary crystalline size was calculated for W and β-W using the Scherrer's equation.

using a sequential incipient wetness impregnation method. First, the support was impregnated with an aqueous solution of ammonium metatungstate hydrate [$(NH_4)_6H_2W_{12}O_{40}{\cdot}xH_2O$, Aldrich] and the catalyst was dried at 393 K overnight. Second, the dried catalyst was again impregnated with an aqueous solution of nickel nitrate hexahydrate [$Ni(NO_3)_2{\cdot}6H_2O$, Junsei Chemical Co.] and dried at 393 K overnight. The Ni and W content were intended to be 5 wt.%, and 25 wt.%, respectively. All the catalysts were reduced in a H_2 stream at 973 K for 1 h and passivated with 1% O_2 in He stream for 1 h at room temperature before the reaction and characterization, unless explicitly specified. In order to control the particle size of the supported tungsten metal in Ni/W/SiO_2(40), the catalyst was reduced in a H_2 stream at different temperatures (viz., 673 K, 773 K, 873 K, 973 K, 1073 K, and 1173 K) for 1 h before the reaction. Ni supported on SiO_2(40) was also prepared using an incipient wetness impregnation method to obtain the 5 wt.% Ni content. Ni/SiO_2(40) catalyst was reduced in a H_2 steam at 873 K for 1 h before the reaction.

Three Ni/W/SiO_2(40) catalysts with different oxidation degrees were also prepared. The reduced Ni/W/SiO_2(40) catalyst (hereby denoted as Ni/W/SiO_2(R)) was reduced in a H_2 steam at 873 K. The passivated Ni/W/SiO_2(40) catalyst (hereby denoted as Ni/W/SiO_2(P)) was prepared by bringing Ni/W/SiO_2(R) into contact with 1% O_2 in He stream for 13 h at room temperature. The oxidized Ni/W/SiO_2(40) catalyst (hereby denoted as Ni/W/SiO_2(O)) was prepared by bringing Ni/W/SiO_2(R) into contact with air for 1 h at 873 K.

2.2. Catalyst characterization

The Brunauer–Emmett–Teller (BET) surface area was calculated based on N_2 adsorption–desorption data obtained using an ASAP 2020 unit (Micromeritics) at liquid N_2 temperature. Prior to the measurement, the sample was degassed under vacuum for 6 h at 473 K. The pore-size distributions for each catalyst were calculated by the Barret–Joyner–Hallender (BJH) desorption method.

The Ni and W content for all the prepared catalysts were analyzed by inductively coupled plasma-atomic emission spectroscopy (ICP-AES, JY-70Plus, Jobin-Yvon) and is listed in Table 1.

The bulk crystalline structures of the catalysts were determined by X-ray diffraction (XRD). The XRD patterns were obtained with a Rigaku D/MAC-III instrument operated at 50 kV and 30 mA using Cu Kα radiation. The crystalline phases were assigned using PCPDFWIN software (version 2.2) for the ICDD database.

The primary crystallite sizes of the catalysts were determined using Scherrer's equation,

$$L = \frac{0.9\lambda_{k\alpha 1}}{B_{(2\theta)}\cos\theta_{\max}} \quad (1)$$

where L denotes the average particle size, 0.9 is the value in radians when $B_{(2\theta)}$ is the full width at half maximum (FWHM) of peak broadening, $\lambda_{K\alpha 1}$ is the wavelength of the X-ray radiation (0.15406 nm), and θ_{max} is the angular position at the (2 0 0) peak maximum of W, and the (2 1 1) peak maximum of β-W.

The temperature-programed desorption of ammonia (NH_3-TPD) was conducted in an AutoChem 2910 unit (Micromeritics) equipped with a thermal conductivity detector (TCD) to measure the NH_3 desorption. A quartz U-tube reactor was loaded with 0.10 g sample, and the catalysts were pretreated in He at the reduction temperature and then cooled to 423 K. The charged sample was treated in 3 vol.% NH_3/He at 423 K for 30 min, and the catalyst was then flushed with He for 1 h. The NH_3-TPD process was performed using 30 mL/min of He by heating the sample at a heating rate of 5 K/min while monitoring the TCD signals. The amount of acid sites was quantified from the NH_3-TPD profile based on the TPD peak area obtained after injecting a known amount of NH_3. In the case of Ni/W/SiO_2(40) catalyst reduced at 673 K, the amount of acid sites were determined from the difference between the TPD profile obtained without NH_3 adsorption and the typical NH_3-TPD profile so as to remove any interference of adsorbed H_2O.

The surface composition of Ni/W/SiO_2(R), Ni/W/SiO_2(P), and Ni/W/SiO_2(O) was analyzed by X-ray photoelectron spectroscopy (XPS) on a K-alpha spectrometer (Thermo Electron, USA) with an Al Kα X-ray source (1486.6 eV photons). The C1s peak at 285 eV was used as the reference for all binding energies. The photo-peak area was determined after the subtraction of the linear spectral background. The spectral simulations were based on a Gaussian profile.

Hydrogen chemisorption was carried out for Ni/SiO_2(40) using a static volumetric apparatus (Mircromeritics ASAP 2020 C). The catalyst was pretreated in vacuum at 393 K for 1 h, and the sample was heated to the reduction temperature of 873 K in flowing H_2. After reduction at 873 K for 2 h, the sample was evacuated at the same temperature for 30 min. The H_2 adsorption isotherms were measured at 308 K. The amount of chemisorbed H_2 at zero pressure was determined via extrapolating the linear part of the isotherm.

2.3. Catalytic performance tests

The relative crystallinity of cellulose (Aldrich, microcrystalline) was estimated by XRD analysis and was as high as 84% [27]. The direct conversion of cellulose into polyols was carried out in a batch reactor. First, 500 mg cellulose and 50 mg catalysts were mixed with 30 mL deionized water; the resulting mixture was introduced into an 85-mL stainless-steel autoclave. The reactor was filled with H_2, and the pressure was fixed at 6 MPa at ambient temperature. The reaction mixture was mixed well at a rate of 700 rpm using a magnetic stirrer; the reaction temperature was attained after 1 h. The zero reaction time was regarded as the time when the temperature reached the set temperature. After the reaction, the autoclave was cooled to room temperature within 0.5 h, and the solid residues were separated from the liquid products by centrifugation. The liquid product was filtered with a 0.2-μm membrane filter and analyzed with a high-performance liquid chromatograph (YL 9110

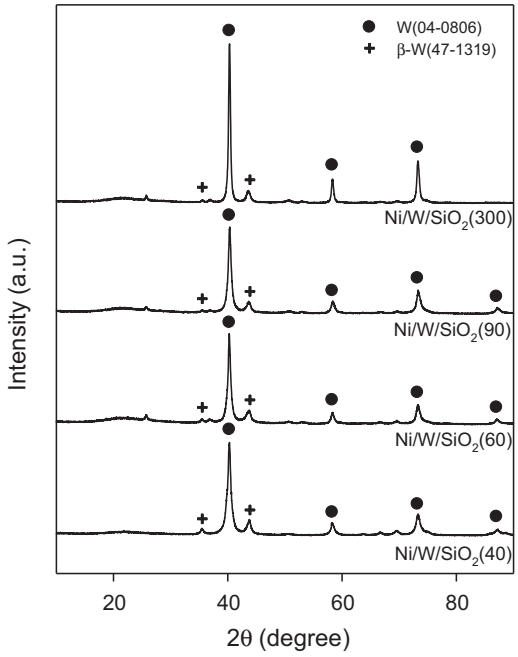

Fig. 1. XRD patterns of Ni/W/SiO_2 with different average pore diameters, viz. 40, 60, 90, and 300 Å. All the catalysts were reduced in H_2 at 973 K and passivated with a stream composed of 1% O_2 in He for 1 h at room temperature.

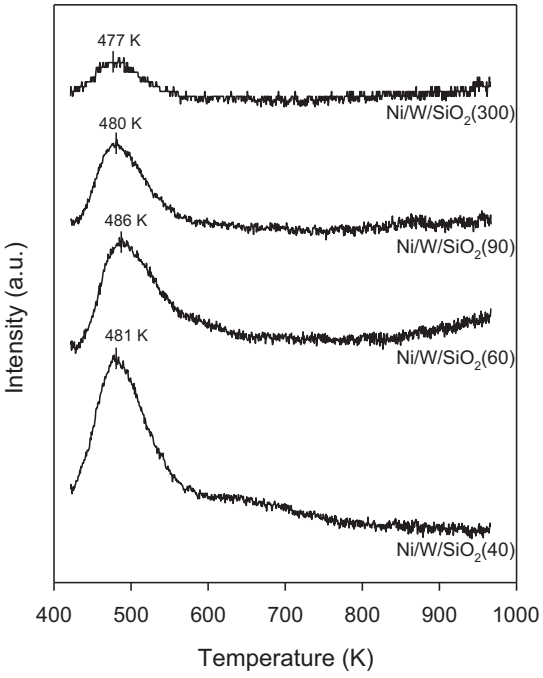

Fig. 2. Temperature-programed desorption of ammonia (NH_3-TPD) patterns of Ni/W/SiO_2(40), Ni/W/SiO_2(60), Ni/W/SiO_2(90), and Ni/W/SiO_2(300). All the catalysts were reduced in H_2 at 973 K and passivated with a stream composed of 1% O_2 in He for 1 h at room temperature.

quaternary pump) equipped with a refractive index detector (YL 9170 RI detector).

The solid product was washed several times with deionized water and dried overnight at 353 K under vacuum to evaluate the cellulose conversion. The cellulose conversion and the product yield were calculated using the following formulae:

$$X_R(\%) = \frac{(M_{R_0} - M_R)}{M_{R_0}} \times 100 \quad (2)$$

$$Y_P(\%) = \frac{M_P}{(M_{R_0} \times y_C)} \times 100 \quad (3)$$

where X_R is the cellulose conversion, M_{R_0} is the weight of cellulose before the reaction, M_R is the weight of cellulose after the reaction, Y_P is the product yield, M_P is the weight of carbon in the product that can be calculated by considering the number of carbon atoms in the product, and y_C is the weight fraction of carbon in cellulose determined via the CHN analysis [27].

3. Results and discussion

3.1. Physicochemical properties of prepared catalysts

Table 1 shows the physicochemical properties of the prepared Ni/W/SiO_2 catalysts with different average pore sizes (40 Å, 60 Å, 90 Å, and 300 Å). The Ni and W loadings in each catalyst were confirmed as 5 wt.% and 25 wt.%, respectively. The BET surface area of the prepared catalyst decreased to approximately half of that of each support. However, as shown in Fig. S1, the pore-size distribution of the prepared catalyst did not undergo much change compared to that of each support.

The XRD patterns of Ni/W/SiO_2 catalysts with different average pore sizes are presented in Fig. 1. All of the catalysts exhibited distinct XRD peaks associated with W (JCPDS No. 04-0806) and β-W (JCPDS No. 47-1319). β-W, which contains a small amount of oxygen, is a metastable form of α-W that decomposes into W and WO_2 above 973 K [28]. The XRD data indicated that a majority of W species are present as reduced form in the final catalyst. No distinct peak related to the Ni species was observed for any of the Ni/W/SiO_2 catalysts containing ~5 wt.% Ni, thus implying that the Ni species were well dispersed on the support. Because the XRD peak intensity is closely related to the crystalline size of the corresponding particle, the crystalline sizes of W and β-W were calculated using Scherrer's equation, and the results are shown in Table 1. The primary crystalline size of W generally increased on increasing the average pore size of support. However, the crystalline size of β-W for each catalyst was similar and ranged from 9.7 to 11.7 nm, irrespective of the average pore size of support.

The NH_3-TPD was carried out to ascertain any change in the acidity of Ni/W/SiO_2 catalysts with different average pore diameters, and the NH_3-TPD profiles are shown in Fig. 2. All the catalysts showed similar TPD pattern, where the maximum peak was observed at 480 K and no noticeable TPD peak was found above 600 K. Because the peak position in the NH_3-TPD profile is directly related to the acid strength, it can be inferred that all the catalysts have similar acid strength and that the acids are not strong. However, the peak intensity appeared to decrease on increasing the average pore diameter of the catalyst. Because the peak intensity in the NH_3-TPD profile is directly related to the acid amount, a quantitative analysis of the NH_3-TPD profile was made and its result is listed in Table 1. The results clearly support the hypothesis that the acid amount of Ni/W/SiO_2 catalysts decrease on increasing the average pore diameter of a catalyst.

Table 2 shows the physicochemical properties of the prepared Ni/W/SiO_2(40) catalysts reduced at different temperatures (673 K, 773 K, 873 K, 973 K, 1073 K, and 1173 K). Although a wide range of reduction temperatures were applied, no significant changes in the BET surface area and pore-size distribution were observed, as shown in Table 2 and Fig. S2. On the other hand, the XRD patterns of the catalysts in Fig. 3 show that the peak intensity corresponding to W and β-W increases on increasing the reduction temperature, thus confirming the results shown in Table 2. In the case of the Ni/W/SiO_2(40) catalyst reduced at 673 K, weak XRD peaks owing to ammonium metatungstate were observed, which

Table 2
Physicochemical properties of Ni/W/SiO_2(40) reduced at different temperatures.

Reduction temperature (K)	BET surface area (m^2/g)	Amount of desorbed NH_3 (μmol NH_3/g)[a]	Particle size (nm)[b]	
			W	β-W
1173	204	8.0	94.3	25.4
1073	202	32.1	37.7	14.8
973	184	78.5	15.5	11.7
873	263	82.1	8.3	11.1
773	250	152.5	–	3.7

[a] The total acidity was determined by quantifying the desorbed NH_3 by NH_3- TPD.
[b] The primary crystalline size was calculated for W and β-W using the Scherrer's equation.

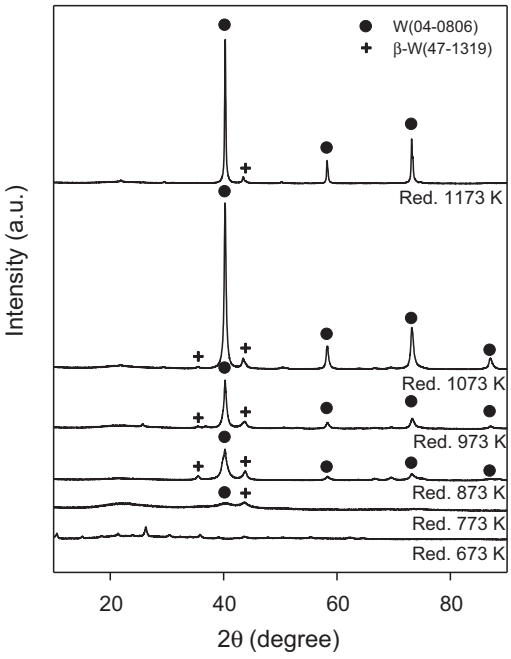

Fig. 3. XRD patterns of Ni/W/SiO_2(40) catalysts reduced in H_2 at different temperatures, viz. 673, 773, 873, 973, 1073, and 1173 K.

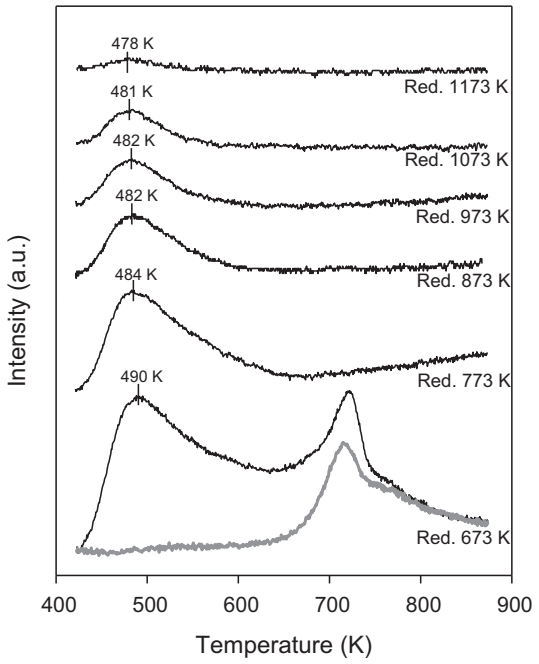

Fig. 4. Temperature-programed desorption of ammonia (NH_3-TPD) patterns (solid line) for Ni/W/SiO_2(40) catalysts reduced in H_2 at different temperatures, viz. 673, 773, 873, 973, 1073, and 1173 K. TPD pattern for Ni/W/SiO_2(40) catalysts reduced in H_2 at 673 K without ammonia adsorption is presented as a gray line.

implied that complete reduction was not achieved at 673 K [29]. The NH_3-TPD process was carried out to find out the surface acidity of Ni/W/SiO_2 catalysts reduced at different temperatures, and the results are shown in Fig. 4. All the catalysts showed similar TPD patterns, where a maximum peak was observed at approximately 480 K and no noticeable TPD peak was found above 600 K. Thus, all the catalysts have a similar acid strength that is not strong. However, the peak intensity appeared to decrease with increasing reduction temperature. The quantitative analysis of the NH_3-TPD profile was carried out and its result is listed in Table 2. For Ni/W/SiO_2(40) reduced at 673 K, the amount of acid sites was calculated to be 415 μmol/g_{cat}. This result clearly supports the fact that the acid amount of Ni/W/SiO_2(40) catalysts decrease on increasing the reduction temperature.

Figure 5 shows the XRD patterns for Ni/W/SiO_2(40) catalysts with different oxidation degrees, viz. Ni/W/SiO_2(R), Ni/W/SiO_2(P), and Ni/W/SiO_2(O). No XRD peak relating to Ni species was observed for all the catalysts, which implied that the Ni species is well dispersed on the support. However, different W species were observed for each catalyst: Ni/W/SiO_2(R) had a well-developed W and β-W. Ni/W/SiO_2(P) had WO_2 crystallite as well as W and β-W whose peak intensities were slightly decreased owing to their transformation into WO_2 as compared to Ni/W/SiO_2(R). Ni/W/SiO_2(O) had WO_3 crystallite only. The surface acidity for these catalysts was probed using NH_3-TPD, as shown in Fig. 6. All the catalysts showed a similar TPD pattern, where a maximum peak was observed at approximately 484 K and no noticeable TPD peak can be found above 600 K, which implied that all catalysts have similar weak acid sites. The total amount of surface acid site for each catalyst was quantified and determined to be 82, 103, and 92 μmol/g_{cat} for Ni/W/SiO_2(R), Ni/W/SiO_2(P), and Ni/W/SiO_2(O), respectively. In order to obtain information about the surface-oxidation state of Ni and W, the Ni2p and W4f XP spectra, as presented in Fig. 7, were obtained for Ni/W/SiO_2(R), Ni/W/SiO_2(P), and Ni/W/SiO_2(O). The W4f XP spectra consisted of two overlapping doublets at binding energies 31.1–35.7 eV for the $W4f_{7/2}$ and 37.7 eV for the $W4f_{5/2}$ lines of W^0, W^{4+}, and W^{6+}. Deconvolution was carried out by fixing $4f_{7/2}$ binding energy for W^0, W^{4+}, and W^{6+} at 31.2, 33.4, and 35.7 eV, respectively. The individual peak had an FWHM of 0.8–1.5 eV. The Ni2p XP spectra exhibited two peaks at 853.2 and 856.6 eV representing Ni and NiO, respectively. A characteristic feature of the Ni2p spectrum was the shake-up satellite at 862–863 eV owing to a charge-transfer transition. The deconvolution yielded peaks with FWHM of 1.6–3.3 eV at 853.3 and 856.7 eV. The quantitative analysis result for the XP spectra is listed in Table 3. The fraction of the metallic Ni and W in the catalyst decreased in the following order: Ni/W/SiO_2(R) > Ni/W/SiO_2(P) > Ni/W/SiO_2(O). It is worth mentioning that a certain fraction of Ni and W existed as oxidized form in the Ni/W/SiO_2(R) catalyst, thus implying that the metallic Ni and W can be oxidized in the passivation step at room temperature. Since

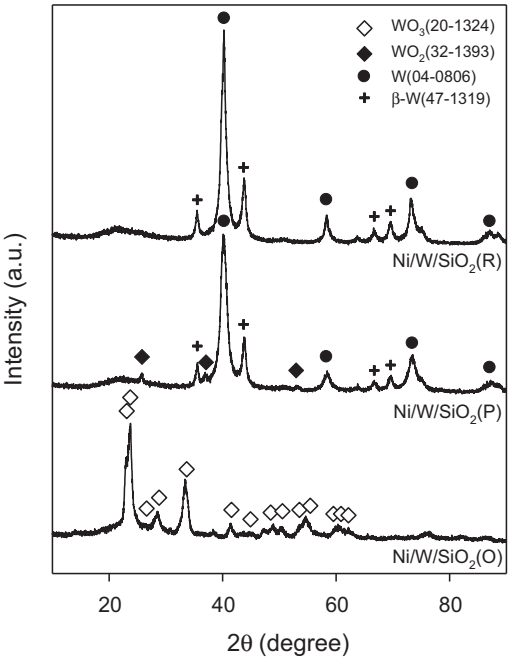

Fig. 5. XRD patterns of Ni/W/SiO_2(40) catalysts with different preparation methods, viz. Ni/W/SiO_2(R), Ni/W/SiO_2(P), Ni/W/SiO_2(O).

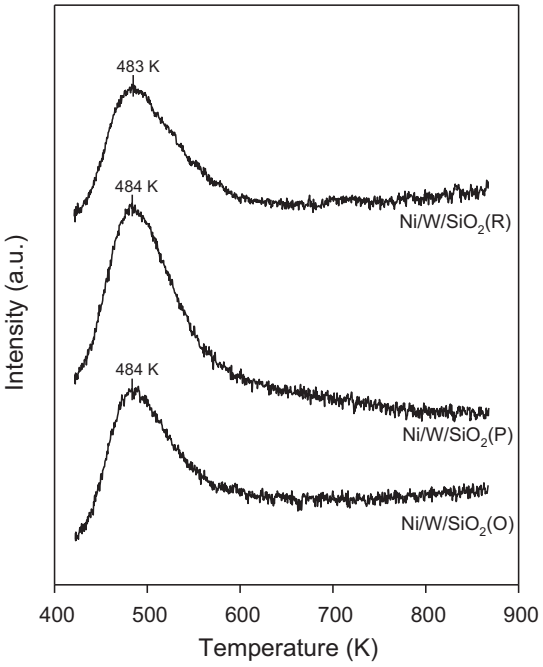

Fig. 6. Temperature-programed desorption of ammonia (NH_3-TPD) patterns for Ni/W/SiO_2(40) catalysts pretreated at different conditions, viz. Ni/W/SiO_2(R), Ni/W/SiO_2(P), and Ni/W/SiO_2(O).

the fraction of W metal in Ni/W/SiO_2(R) was higher than that of Ni/W/SiO_2(P), it can be inferred that the surface oxidation of Ni and W is time-dependent. In the case of Ni/W/SiO_2(O) catalyst, only W^{6+} and Ni^{2+} were confirmed to be present as W and Ni species on the catalyst surface. Based on XRD and XPS data, it can be said that the bulk crystalline W metal is covered with a certain fraction of WO_2 and WO_3 in Ni/W/SiO_2(R) and Ni/W/SiO_2(P). Moreover, the surface tungsten oxides can act as acid sites for this reaction. This is quite reasonable because the catalyst with smaller W particles can have a larger amount of surface acid sites as long as the same amount of W is loaded and the same fraction of surface is oxidized. This is consistent with the present results where the catalyst with the largest W metal particles prepared on a support with large average pore diameter or prepared through a reduction step at high temperatures has a small amount of surface acid sites.

3.2. Effect of crystalline size of W metal

The direct conversion of cellulose into various polyols such as sorbitol, mannitol, erythritol, ethylene glycol, and 1,2-propanediol in the presence of H_2 over Ni/W/SiO_2 catalysts was carried out

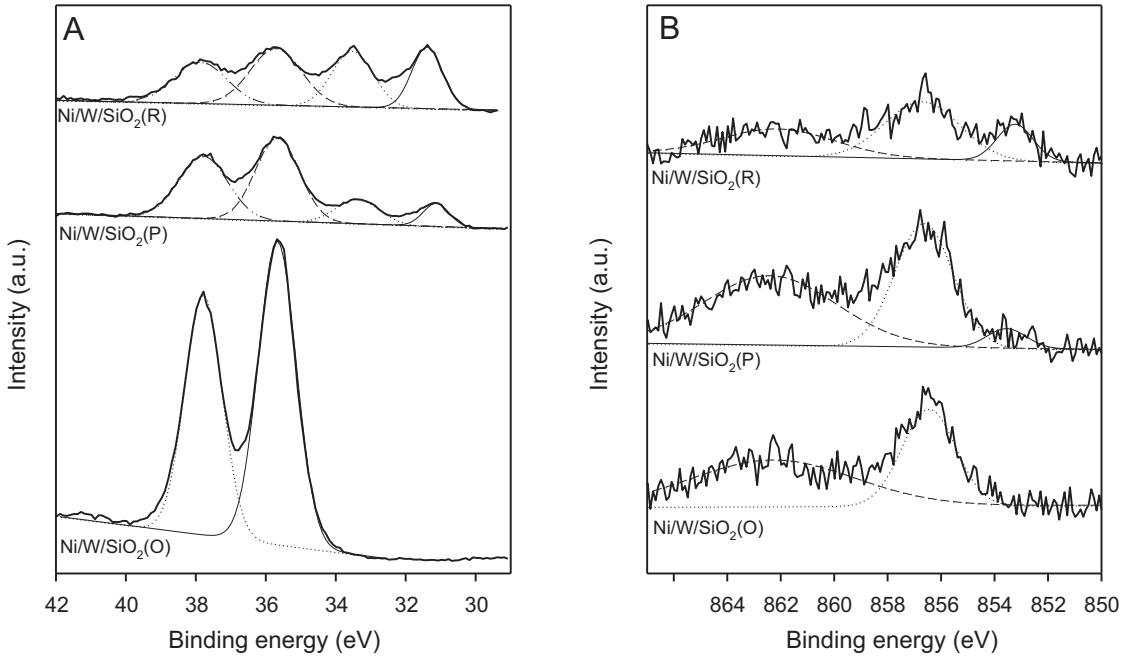

Fig. 7. X-ray photoelectron spectra of (A) W4f region and (B) Ni2p core-level depicting photoelectron peak of Ni/W/SiO_2(40) catalysts pretreated at different conditions, viz. Ni/W/SiO_2(R), Ni/W/SiO_2(P), and Ni/W/SiO_2(O).

Table 3
Surface composition of W and Ni species in Ni/W/SiO_2(40) catalysts pretreated at different conditions.

Catalysts	% Contribution of $W4f_{7/2}$			% Contribution of $Ni2p_{3/2}$	
	W	WO_2	WO_3	Ni	NiO
Ni/W/SiO_2(R)	29.9	31.2	38.9	23.3	76.7
Ni/W/SiO_2(P)	14.0	19.7	66.3	9.6	90.4
Ni/W/SiO_2(O)	–	–	100	–	100

Table 4
Cellulose conversion and polyol selectivities in presence of various catalysts.[a,b]

Catalysts	Conversion (%)	Selectivity (%)				
		Sorbitol	Mannitol	Erythritol	Ethylene glycol	1,2-Propanediol
Ni/W/SiO_2(40)	81 (94)	2.7 (2.8)	0.5 (1.2)	1.4 (1.9)	22.9 (24.7)	4.8 (5.2)
Ni/W/SiO_2(60)	80 (91)	3.4 (5.2)	0.6 (2.0)	1.3 (2.1)	23.0 (20.2)	5.0 (8.9)
Ni/W/SiO_2(90)	79 (95)	3.3 (4.3)	0.9 (1.6)	0.8 (2.2)	12.5 (18.7)	5.4 (8.6)
Ni/W/SiO_2(300)	83 (94)	3.2 (4.9)	0.9 (1.7)	0.8 (1.6)	10.9 (14.6)	6.9 (8.9)
Ni/W/SiO_2(40) R1173 K	80 (100)	2.3 (2.6)	0.7 (0.9)	1.0 (1.2)	14.8 (13.0)	4.0 (4.4)
Ni/W/SiO_2(40) R1073 K	79 (100)	2.7 (3.0)	0.5 (1.1)	1.1 (2.0)	16.9 (19.8)	4.6 (4.8)
Ni/W/SiO_2(40) R873 K	81 (99)	2.3 (1.9)	0.5 (1.8)	1.6 (1.9)	26.8 (30.2)	5.1 (6.8)
Ni/W/SiO_2(40) R773 K	80 (100)	1.7 (3.1)	0.6 (2.1)	1.6 (1.8)	25.1 (29.9)	5.0 (7.0)
Ni/W/SiO_2(40) R673 K	85 (100)	1.2 (0.6)	0.6 (0.6)	1.4 (1.3)	12.7 (10.3)	2.2 (2.7)

[a] Reaction conditions: weight of cellulose = 500 mg; volume of water = 30 mL; weight of catalyst = 50 mg; reaction temperature = 518 K; reaction time = 1 h; and initial H_2 pressure = 6 MPa.
[b] Data in parentheses were obtained after 2 h of reaction.

and the catalytic performance is summarized in Table 4. In this study, a much smaller amount of catalysts (cellulose/metal ratio of 33 (w/w)) is used in comparison to the previous works (cellulose/metal ratio of 5–21 (w/w)) [19–25].

83% cellulose conversion was achieved after 2 h at 518 K even in the absence of any catalyst because of the unique properties of hot water [30]. However, no detectable amount of polyols was obtained. In the presence of Ni/W/SiO_2 catalysts, the cellulose conversions and polyols yields were above 80% and 20%, respectively, after 1 h. They increased to be above 90% and 30%, respectively, after 2 h. Among the polyols, ethylene glycol and 1,2-propanediol are the main products. Traces of sorbitol, mannitol, and erythritol were also detected. Most of the peaks detected by HPLC were identified. The other unidentified products could be gaseous compounds (CO_2, CO, H_2, and alkanes), soluble oligosaccharides, and polymers.

Among Ni/W/SiO_2 catalysts with different average pore diameters, the Ni/W/SiO_2(40) catalyst showed the highest ethylene glycol selectivity of 25%, which increased on decreasing the average pore size of the catalyst. However, no noticeable difference was found in the product distribution among these catalysts.

The catalytic activity was compared among the Ni/W/SiO_2(40) catalysts reduced at different temperatures. The ethylene glycol yield was dependent on the reduction temperature and decreased in the following order: 873 K ~ 773 K > 973 K > 1073 K > 1173 K > 673 K. The same trend was observed for 1,2-propanediol yield. As shown in Section 3.1, the Ni/W/SiO_2(40) catalyst reduced at 673 K was not completely reduced although it had the largest surface acid amount. This implied that the catalytic activity is inversely proportional to the crystal size of W as long as the catalyst was completely reduced, as shown in Fig. 8.

The effect of the reaction time on the hydrogenolysis of cellulose into polyols was examined over Ni/W/SiO_2(40) reduced at 973 K, as shown in Fig. S3. The cellulose conversion increased with increasing reaction time and the polyol selectivity increased continuously with increasing reaction time till 8 h. These results imply that polyols don't undergo severe degradation to by-products under these typical reaction conditions.

To examine the catalyst stability under the reaction conditions, the concentration of W in the liquid phase was quantified by

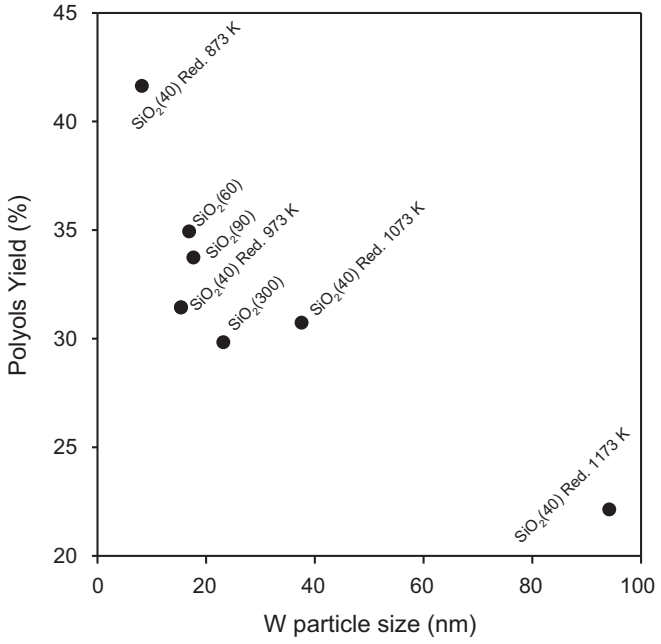

Fig. 8. Polyol yields and particle size of W correlations as determined by XRD for Ni/W/SiO_2.

ICP-AES after the reaction and was determined to be 180 ppm, corresponding to 34.84% of W content in the fresh catalyst. To find out any change in the structure and electronic state of Ni and W species during the reaction, XRD and XPS analysis were carried out for Ni/W/SiO_2(40) reduced at 873 K catalysts after a reaction. As shown in Fig. S4, the XRD peak intensity due to W decreased considerably and peaks corresponding to β-W disappeared. On the other hand, new XRD peaks due to WO_3 appeared after a reaction. W4f and Ni2p spectra in Fig. S5 also clearly support that Ni and W were oxidized during the reaction. Therefore, it can be concluded that the metal leaching and surface oxidation are main causes of catalyst deactivation for this reaction. The catalyst deactivation in the liquid-phase organic reactions was reported to be dependent on

Table 5
Cellulose conversion and polyol yields in the presence of various catalyst systems.

Catalysts	Conversion (%)	Yield (%)				
		Sorbitol	Mannitol	Erythritol	Ethylene glycol	1,2-Propanediol
$Ni/W/SiO_2(R)$[a]	99	1.9	1.8	1.9	29.9	6.1
$Ni/W/SiO_2(P)$[a]	100	2.8	0.7	1.7	26.7	5.4
$Ni/W/SiO_2(O)$[a]	100	–	–	–	–	–
$Ni/SiO_2(40)+W$[b]	100	1.2	0.4	0.7	2.6	0.7
$Ni/SiO_2(40)+WO_3$[b]	100	0.6	0.1	0.9	2.7	0.3

[a] Reaction conditions: weight of cellulose = 500 mg; volume of water = 30 mL; weight of catalyst = 50 mg; reaction temperature = 518 K; reaction time = 2 h; and initial H_2 pressure = 6 MPa.
[b] Reaction conditions: weight of cellulose = 500 mg; volume of water = 30 mL; weight of nickel catalyst = 50 mg; weight of tungsten catalyst = 50 mg; reaction temperature = 518 K; reaction time = 2 h; and initial H_2 pressure = 6 MPa.

solvent properties (pH, oxidation potential, chelating properties of molecules) and the bulk properties and surface properties of the solid catalyst [31].

3.3. Effect of degree of surface oxidation

The catalytic activity compared among the various $Ni/W/SiO_2(40)$ catalysts with different surface oxidation degrees is shown in Table 5. The highest polyols yield was obtained over $Ni/W/SiO_2(R)$. The polyol yield increased with increasing fraction of the metallic Ni and W. The product distribution was dependent on the fraction of the metallic Ni and W. The yields of ethylene glycol, lactic acid, and acetic acid were 30%, 0%, and 0%, respectively, over $Ni/W/SiO_2(R)$, while they were 0%, 22%, and 3%, respectively, over $Ni/W/SiO_2(O)$. An explanation for the varying yields is that the $Ni/W/SiO_2(R)$ catalyst containing reduced and oxidized Ni and W species is effective for the hydrogenolysis of cellulose into low-molecular-weight polyols. On the other hand, $Ni/W/SiO_2(O)$ catalyst containing only oxidized Ni and W species produces organic acids via a series of reactions such as hydrolysis, elimination, and rearrangement [32]. Chambon et al. [33] carried out cellulose conversion using solid acids and obtained high yields of lactic acid, levulinic acid, and formic acid.

The hydrogenolysis of cellulose into polyols involves C-C bond cleavage and C—O bond cleavage via dehydrogenation, retro-aldol condensation, decarbonylation, dehydration, hydrogenation [34,35]. The key steps in C—C bond cleavage are dehydrogenation, decarbonylation, and retro-aldol condensation at metal sites [35]. Dehydration is effective at C—O bond cleavage on acid sites, and hydrogenation occurs on metal site [35]. For $Ni/W/SiO_2$ catalysts, metallic tungsten, oxidized tungsten, and metallic nickel are responsible for C—C bond cleavage, C—O bond cleavage, and hydrogenation, respectively. That's why the balance and location of metal site and acid site are critical to increase polyols yields.

In our previous work [26], the hydrogenolysis of cellulose over $Ni/W/SiO_2$-Al_2O_3 catalysts was examined. In $Ni/W/SiO_2$-Al_2O_3 catalysts, a large amount of acid sites of SiO_2-Al_2O_3 causes smaller W particle size and larger amount of acid sites, compared with $Ni/W/SiO_2$ catalysts in this study. Although $Ni/W/SiO_2$-Al_2O_3 catalysts have smaller W particle size than $Ni/W/SiO_2$ catalysts, these catalysts provide lower polyols yield owing to lots of acid sites. This implies that $Ni/W/SiO_2$ catalysts have more proper balance of metal site and acid site than $Ni/W/SiO_2$-Al_2O_3 ones.

To understand the synergistic effect of Ni and W in this reaction, the combined catalyst systems composed of $Ni/SiO_2(40)$ and W species (W or WO_3) were compared under the same reaction conditions (Table 5). The amount of chemisorbed H_2 for $Ni/SiO_2(40)$ was determined to be 13.1 $\mu mol/g_{cat}$, which corresponds to 3.1% Ni dispersion. In both the cases, the total yield to polyols was 5–6%. The lactic acid yield was 7% and 15% for Ni/SiO_2 + W and Ni/SiO_2 + WO_3 systems, respectively, indicating that NiW bimetallic catalyst had a remarkable synergistic effect on the hydrogenolysis of cellulose.

Thus, based on the previous and present data, the following reaction scheme can be considered, where first, cellulose is hydrolyzed into glucose/oligosaccharide by H^+ ions generated in hot water. The formed sugar intermediates can then be transformed into low-molecular-weight polyols over reduced NiW bimetallic catalysts through hydrogenolysis in a H_2-rich atmosphere. In the presence of fully oxidized tungsten oxides, the sugar intermediates can then be transformed into organic acids via a series of reactions such as hydrolysis, elimination, and rearrangement [32].

4. Conclusion

The primary crystalline size of W increased on increasing the average pore size of support and reduction temperature for the $Ni/W/SiO_2$ catalysts containing 5 wt.% Ni and 25 wt.% W. However, the amount of surface acid site decreased on increasing the average pore size of support and reduction temperature. A certain fraction of Ni and W can be oxidized in the passivation step at room temperature. Therefore, the bulk crystalline W metal is covered with a certain fraction of WO_2 and WO_3 in $Ni/W/SiO_2$ catalysts. The catalytic activity is inversely proportional to the crystal size of W metal. A $Ni/W/SiO_2$ catalyst containing reduced and oxidized Ni and W species is effective for the hydrogenolysis of cellulose into low-molecular-weight polyols. On the other hand, a $Ni/W/SiO_2$ catalyst containing only oxidized Ni and W species produces organic acids via a series of reactions such as hydrolysis, elimination, and rearrangement. The combined catalyst systems comprising Ni/SiO_2 and W species (W or WO_3) showed lower polyol yields compared to the $Ni/W/SiO_2$ catalysts, thus indicating that the NiW bimetallic catalyst has a remarkable synergistic effect on the hydrogenolysis of cellulose.

Acknowledgements

This work was financially supported by a grant from the Industrial Source Technology Development Programs (10033099) of the Ministry of Knowledge Economy (MKE), Republic of Korea.

Appendix A. Supplementary data

Supplementary data associated with this article can be found, in the online version, at http://dx.doi.org/10.1016/j.apcata.2013.06.053.

References

[1] G.W. Huber, S. Iborra, A. Corma, Chem. Rev. 106 (2006) 4044–4098.
[2] M. FitzPatrick, P. Champagne, M.F. Cunningham, R.A. Whitney, Bioresour. Technol. 101 (2010) 8915–8922.
[3] R. Rinaldi, F. Schüth, Energy. Environ. Sci. 2 (2009) 192–196.
[4] A. Fukuoka, P.L. Dhepe, Angew. Chem. Int. Ed. 45 (2006) 5161–5163.

[5] S.J. You, I.G. Baek, Y.T. Kim, K.-E. Jeong, H.-J. Chae, T.-W. Kim, C.-U. Kim, S.-Y. Jeong, T.J. Kim, Y.-M. Chung, S.-H. Oh, E.D. Park, Korean J. Chem. Eng. 28 (2011) 744–750.
[6] H. Kobayashi, Y. Ito, T. Komanoya, Y. Hosaka, P.L. Dhepe, K. Kasai, K. Hara, A. Fukuoka, Green Chem. 13 (2011) 326.
[7] M. Käldström, N. Kumar, D.Y. Murzin, Catal. Today 167 (2011) 91–95.
[8] C. Luo, S. Wang, H. Liu, Angew. Chem. Int. Ed. 46 (2007) 7636–7639.
[9] H. Wang, L. Zhu, S. Peng, F. Peng, H. Yu, J. Yang, Renew. Energy 37 (2011) 192–196.
[10] W. Deng, X. Tan, W. Fang, Q. Zhang, Y. Wang, Catal. Lett. 133 (2009) 167–174.
[11] M. Liu, W. Deng, Q. Zhang, Y. Wang, Y. Wang, Chem. Commun. 47 (2011) 9717–9720.
[12] J. Geboers, S. Van de Vyver, K. Carpentier, K. de Blochouse, P. Jacobs, B. Sels, Catal. Commun. 46 (2010) 3577–3579.
[13] R. Palkovits, K. Tajvidi, A.M. Ruppert, J. Procelewska, Catal. Commun. 47 (2011) 576–578.
[14] G. Liang, C. Wu, L. He, J. Ming, H. Cheng, L. Zhuo, F. Zhao, Green Chem. 13 (2011) 839–842.
[15] R. Palkovits, K. Tajvidi, J. Procelewska, R. Rinaldi, A. Ruppert, Green Chem. 12 (2010) 972–1112.
[16] J. Geboers, S. Van de Vyver, K. Carpentier, P. Jacobs, B. Sels, Catal. Commun. 47 (2011) 5590–5592.
[17] Y. Liu, C. Luo, H. Liu, Angew. Chem. Int. Ed. 51 (2012) 3249–3253.
[18] Z. Tai, J. Zhang, A. Wang, M. Zheng, T. Zhang, Chem. Commun. 48 (2012) 7052–7054.
[19] N. Ji, T. Zhang, M. Zheng, A. Wang, H. Wang, X. Wang, J.G. Chen, Angew. Chem. Int. Ed. 47 (2008) 8510–8513.
[20] Y. Zhang, A. Wang, T. Zhang, Chem. Commun. 46 (2010) 862–864.
[21] M.-Y. Zheng, A.-Q. Wang, N. Ji, J.-F. Pang, X.-D. Wang, T. Zhang, ChemSusChem 3 (2010) 63–66.
[22] X. Wang, L. Meng, F. Wu, Y. Jiang, L. Wang, X. Mu, Green Chem. 14 (2012) 758–765.
[23] G. Liang, H. Cheng, W. Li, L. He, Y. Yu, F. Zhao, Green Chem. 14 (2012) 2146–2149.
[24] J. Pang, A. Wang, M. Zheng, Y. Zhang, Y. Huang, X. Chen, T. Zhang, Green Chem. 14 (2012) 614–617.
[25] L.-N. Ding, A.-Q. Wang, M.-Y. Zheng, T. Zhang, ChemSusChem 3 (2010) 818–821.
[26] I.G. Baek, S.J. You, E.D. Park, Bioresour. Technol. 114 (2012) 684–690.
[27] S.J. You, S.B. Kim, Y.T. Kim, E.D. Park, Clean Technol. 16 (2010) 19–25.
[28] G. Hagg, N. Schonbero, Acta Crystallogr. 7 (1954) 351–352.
[29] M.J.G. Fait, H.J. Lunk, M. Feist, M. Schneider, J.N. Dann, T.A. Frisk, Thermochim. Acta 469 (2008) 12–22.
[30] N. Akiya, P.E. Savage, Chem. Rev. 102 (2002) 2725–2750.
[31] M. Besson, P. Gallezot, Catal. Today 81 (2003) 547–559.
[32] F. Jin, H. Enomoto, Energy Environ. Sci. 4 (2011) 382–397.
[33] F. Chambon, F. Rataboul, C. Pinel, A. Cabiac, E. Guillon, N. Essayem, Appl. Catal. B: Environ. 105 (2011) 171–181.
[34] J.N. Chheda, G.W. Huber, J.A. Dumesic, Angew. Chem. Int. Ed. 46 (2007) 7164–7183.
[35] N. Li, G.W. Huber, J. Catal. 270 (2010) 48–59.